

See discussions, stats, and author profiles for this publication at: <https://www.researchgate.net/publication/41087347>

Hexagonal Lattice Model of the Patterns Formed by Hydrogen-Bonded Molecules on the Surface

ARTICLE *in* THE JOURNAL OF PHYSICAL CHEMISTRY B · FEBRUARY 2010

Impact Factor: 3.3 · DOI: 10.1021/jp9098649 · Source: PubMed

CITATIONS

13

READS

32

3 AUTHORS, INCLUDING:



Sara Fortuna

University of Udine

15 PUBLICATIONS 151 CITATIONS

SEE PROFILE



David L Cheung

National University of Ireland, Galway

54 PUBLICATIONS 995 CITATIONS

SEE PROFILE

Hexagonal Lattice Model of the Patterns Formed by Hydrogen-Bonded Molecules on the Surface

Sara Fortuna,* David L. Cheung,* and Alessandro Troisi*

Department of Chemistry and Centre for Scientific Computing, University of Warwick, Coventry, United Kingdom

Received: October 14, 2009; Revised Manuscript Received: December 17, 2009

We model the two-dimensional self-assembly of planar molecules capable of complementary interactions (like hydrogen bonding) as a set of hexagonal tiles on a hexagonal lattice. We use Monte Carlo simulations to study the phase diagrams of three model systems. The phases are characterized using a variety of order parameters, and they are studied as a function of the strength of the complementary interaction energy. This simplified model is proven to be capable of reproducing the phases encountered in real systems, unifying within the same framework most of the structures encountered experimentally.

1. Introduction

The hydrogen-bond-driven self-assembly of molecular systems adsorbed onto a surface has recently attracted great interest due to the ability of the building blocks to autonomously form nanoscale regular patterns.^{1–3} A variety of systems have been studied, which have been shown to form several two-dimensional structures on surfaces, with common motifs including square^{4,5} and hexagonal networks,^{6–9} lamellar¹⁰ and honeycomb structures,^{11–14} and linear and quasi-linear aggregates.^{15,16} Here, we focus our attention on chemical systems forming hexagonal networks. In a hexagonal network, as the molecular building blocks are often based on aromatic benzene rings (such as benzene-dicarboxylic acids),^{6–8} the underlying symmetry of the molecules often leads to hexagonal networks, with each molecule having six neighbors.

In almost all cases, the molecules interact with their neighbors through hydrogen bonds (H-bonds) and van der Waals interactions (although other interactions, such as π -stacking,⁹ have also been observed), and in Figure 1, we show how it is possible to group the building blocks forming hexagonal networks on the basis of the angular distance between the strongest binding directions. Molecules with 120 or 180° between the H-bonds, such as meta- or para-dicarboxylic acids,^{6–8} are capable of forming compact regular structures (Figure 1b–c), but no regular patterns have been observed if the angular distance between the complementary groups is equal to 60° (Figure 1a), as happens with the phthalic acid.⁶ Interestingly, some systems, even when presenting the same bonding motif, form noncompact structures in which the order is kept only for a few molecular units. Examples include 4-phenylazopyridine¹⁷ or CTBPP¹⁸ on Au(111) which self-assembles in trimers (Figure 1d), cytosine on Au(111)¹⁹ which forms chains and rings (Figure 1e), and Br₂–PTCDI on Ag–Si(111)²⁰ that forms fibrillar structures (Figure 1f).

Systems that self-assemble on metallic surfaces have been studied theoretically using a number of methods, such as density functional theory (DFT) or molecular dynamics (MD) and Monte Carlo (MC). Due to the computational cost, DFT has

been restricted to static calculations on small numbers of molecules. DFT calculations have been used to study single molecules^{7,20} and the supramolecular structures formed by small numbers of molecules,^{20–23} considered to be the building blocks of larger scale assemblies.

For instance, the deviation from planarity of a set of dicarboxylic acids is associated with a low adsorption energy of the molecule on the surface,⁷ and the 2D optimization of molecular chains leads to the conclusion that the hydrogen bonds of a two-dimensional system are extended with respect to those formed in a three-dimensional system.²¹ In other studies,^{20,22,23} dimers, trimers, and tetramers of the same molecule have been investigated to identify the lowest energy supramolecular building block; for instance, melamine dimers and tetramers have been studied to identify the structures compatible with the geometry of the Au(111) surface.²³ Mixed *ab initio* and molecular mechanics methods have been used to study the CTBPP on Au(111), using benzonitrile as a model,²⁴ to confirm the experimental structure¹⁸ (Figure 1d).

In general, the effect of the surface on the self-assembled structure has been studied in more detail with MD²⁵ and MC²⁶ simulations with all atom representations; in particular, these have been used to identify the absorption sites on the surface. For instance, MD simulations have been used to follow the motion of DNA nucleobasis on a Au(111) surface to calculate the adsorption energies and the mobility of the molecules²⁵ on the surface. Kinetic Monte Carlo simulated annealing has been used to study oxalic amide derivative assemblies which appear to be templated by the Ag(111) surface properties,²⁶ and to study the patterns formed by PTCDA and melamine on Au(111)²⁷ performing 2D simulations (assuming no effect of the surface other than keeping the structure planar). Phase diagrams have been calculated for mixtures; for example, a thermodynamic equilibrium model has been employed to describe the phases observed experimentally of a mixture of 1,3,5-benzenetribenzoic acid (BTB) and 1,3,5-tricarboxybenzene trimesic acid (TMA),²⁸ and a lattice model for a melamine–PTCDI mixture.²⁹

As the available theoretical studies are in general concerned with the interpretation of specific experimental systems, a general understanding of the relationship between the shape and structure of the building blocks and the supramolecular structure they can form on surfaces is still lacking. This work aims at

* To whom correspondence should be addressed. E-mail: S.Fortuna@warwick.ac.uk (S.F.); David.Cheung@warwick.ac.uk (D.L.C.); A.Troisi@warwick.ac.uk (A.T.).

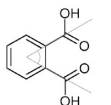
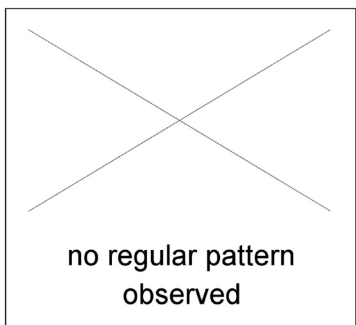
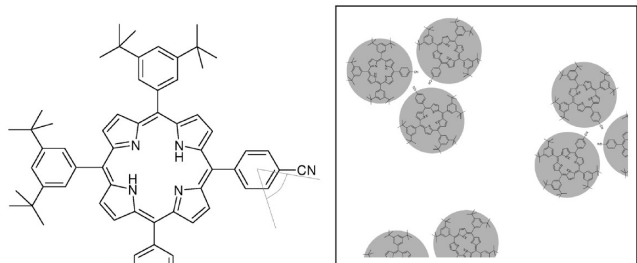
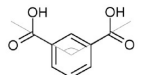
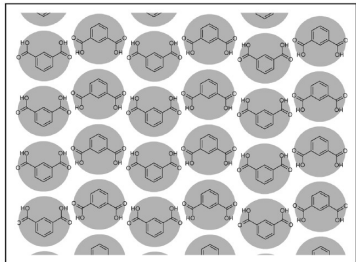
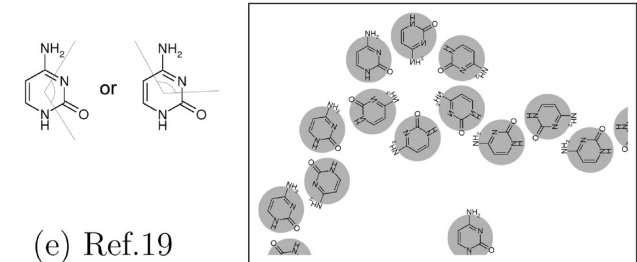
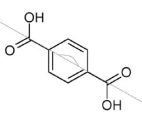
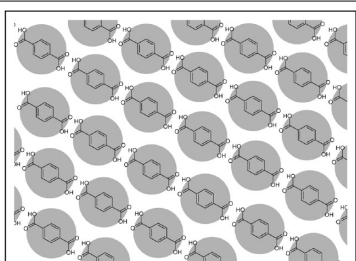
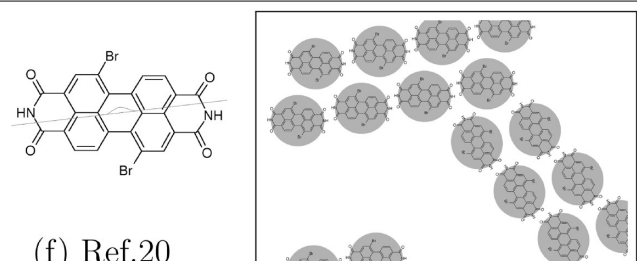
angle	compact		non-compact	
$\sim 60^\circ$	<div></div> <div>(a) Ref.6</div>	<div></div>	<div></div> <div>(d) Ref.18</div>	
$\sim 120^\circ$	<div></div> <div>(b) Ref.6</div>	<div></div>	<div></div> <div>(e) Ref.19</div>	
$\sim 180^\circ$	<div></div> <div>(c) Ref.6</div>	<div></div>	<div></div> <div>(f) Ref.20</div>	

Figure 1. Schematic representation of the two-dimensional structures formed by a representative set of molecules with different angles between the groups with complementary interactions. Compact structures (left) are observed for (a) phthalic acid,⁶ (b) terephthalic acid on graphite⁶ and (c) isophthalic acid on graphite.⁶ Noncompact structures (right) are observed for (d) CTBPP on Au(111),¹⁸ (e) cytosine on Au(111),¹⁹ and (f) Br-PTCDI on AgSi(111).²⁰

building a common framework able to rationalize the broad range of structures that one can form on a planar surface. It has been largely shown that it is possible to construct simplified models that can reveal how the building block structure can affect the phase behavior of a system, as observed in real systems.³⁰ Such simplified models have been used to study a wide range of systems, including liquid crystals,³¹ polymers, and proteins.³² In this context, lattice models, in which only the essential features of real systems are retained, have proven to be particularly useful to describe the rich phase behavior that can be observed experimentally. For example, lattice models have a long history in the study of polymers,³³ for the behaviors of proteins and other biomacromolecules,^{34,35} liquid crystals,^{36,37} and the most stable self-assembled structures that a set of particles can form with agent-based techniques.^{38,39}

Here, due to the particular symmetry of the problem, we will model molecular systems forming hexagonal networks as a set of tiles on a hexagonal lattice. The physical motivation for this choice is that the hexagonal packing is very commonly found in molecules absorbed on surfaces; therefore, it is reasonable to approximate the system as a lattice system with the same symmetry. Hexagonal lattices have been extensively used for the study of the magnetic properties of materials, using both the Ising⁴⁰ and Potts models.⁴¹ In the Ising model, each lattice site can assume one of two states; in the Potts model, the number of states for each site is greater than two (that is why it is also called the multistate Ising model). The Ising model can give us

useful information about the phase transitions of particle systems.⁴² Unfortunately, molecular systems are far more complicated and more detailed models should be developed to study their properties. A step in this direction is the “poker chip model”, used to study the directional ordering of proteins in a 2D hexagonal lattice⁴³ by Higo and collaborators. In their model, each protein is represented as a hexagonal chip. The chips are free to perform discrete rotations, but their position on the lattice is fixed to the lattice points. The interaction between two neighboring chips is described assigning a coefficient to each edge of the chips, and multiplying the coefficients at the contact point to take into account the relative orientations of the two proteins, which affects the interaction strength between the two. The critical behavior of this model has been studied by Hogyoku.⁴⁴ Similar models with continuous degrees of freedom have been used to study the behavior of patchy colloidal particles^{32,45} as models of proteins. A more recent example of the hexagonal lattice model has been proposed by Weber and collaborators, to simulate the self-assembly of a melamine–PTCDI molecular mixture deposited on a metal surface by gas deposition²⁹ using MC in the NVT ensemble. Their model, where the molecules occupy the edges and vertexes of a hexagonal lattice, successfully simulates the self-assembled structure formed by gas deposition.

Here, simulations are carried out in the NVT ensemble, in order to simulate the self-assembled structure formed by planar molecules capable of complementary interaction, such as

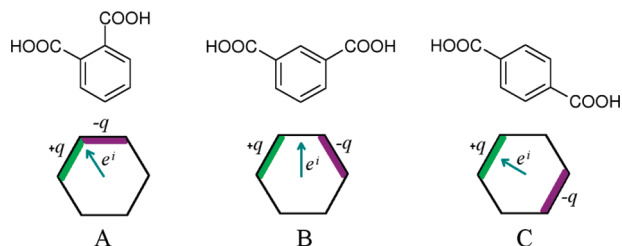


Figure 2. The three different hexagonal tiles considered in this work, building blocks of the self-assembled structures. A tile interacts with other tiles through a van der Waals-like interaction through each edge, plus an electrostatic interaction acting only between the marked edges. The tiles A, B, and C can be thought of as models of the three benzene-dicarboxylic acids with substituents in the ortho, meta, and para positions, respectively. The arrows indicate the vectors e^i relative to the orientation of the tiles with respect to the lattice frame.

hydrogen bonding; unlike ref 29, the molecules of our model occupy the hexagonal sites of the lattice, instead of its edges. Moreover, we will consider systems composed of identical molecules and we will discuss three different classes of molecular systems. In the next section, our hexagonal-lattice model for the hydrogen-bond-driven self-assembly is introduced; then, the structures and phases expressed by the system are identified and analyzed. Finally, the simulation results are discussed in the context of the available experimental data.

2. Model System and Order Parameters

We consider a set of identical non-overlapping hexagonal tiles on a 2D hexagonal lattice with periodic boundary conditions. Adjacent tiles interact with a van der Waals-like interaction plus an additional electrostatic-like contribution, if two charged edges are in contact. Each edge l of a tile i has a formal “charge” $Q_i^{(l)}$ and the Hamiltonian of the system is

$$H = \frac{1}{2} \sum_{\langle ii' \rangle} (-\varepsilon) + \frac{1}{2} \sum_{\langle il, i'l' \rangle} Q_i^{(l)} Q_{i'}^{(l')} \quad (1)$$

where the summation $\langle ii' \rangle$ extends over all adjacent tiles i and i' and the summation $\langle il, i'l' \rangle$ extends only over the contact edges l and l' of the adjacent tiles i and i' . We consider the three charge distributions depicted in Figure 2: in the tile of type A, two consecutive edges are charged with opposite polarity, in the tiles of type B, two nonconsecutive edges are charged with opposite polarity, and in the tiles of type C, the opposite edges are charged. The absolute value of the charge on the charged edges is set to the parameter q . The charged edges can be thought of as donor–acceptor hydrogen-bonding groups, or any group capable of complementary and local interaction. Since the Hamiltonian of the model has the same dimensionality and interaction pattern of the realistic system, it should produce phase diagrams similar to those observed in reality because the corresponding phase transitions should belong to the same universality class.⁴² This is never known a priori, but the fact that the model is able to reproduce several experimental observations suggests that it incorporates the essence of the self-assembly process in these systems.

The model is easy to generalize for more complicated interactions, but in this minimal form, it is already capable of expressing a rich phase behavior. For example, the tiles A, B, and C can be thought of as representing three benzene-dicarboxylic acids with substituents in ortho, meta, and para positions, respectively, systems in which the core of the

molecule is rigid, without large side chains and substituents whose steric effect might significantly affect the packing. In the model, when two opposite charged edges are in contact, we will say they are forming a hydrogen bond (H-bond), and the average number of H-bonds per tile $\bar{\eta}_H$ is a useful measure to characterize the phases expressed by the system.²⁹

We performed Metropolis MC simulations where the tiles are allowed to move on the lattice. The tiles move through attempted translations and rotations (about the C_6 axes orthogonal to the tile) and by flipping about one of the six C_2 axes in the plane of the surface. The latter is a useful move for reaching equilibrium in the simulations, even though if in real systems it is associated to a very high energy barrier and will take place on longer time scales with respect to the other two moves. At each simulation step, a move is randomly performed and accepted with a Metropolis acceptance probability.⁴⁶

On the lattice, each tile i has an associated orientation e^i with respect to the lattice frame (depicted as arrows, in Figure 2). As the tile orientations belong to a discrete set ($e^i \in \{e_n, -e_n\}$, $n = 1, 2, 3$), we can identify the preferred orientation as the most commonly found orientation.⁴⁷ The degree of order may be characterized through the orientational order parameter S . As many of the ordered structures formed by these molecules either involve antiparallel pairs of molecules or are identical when the symmetry axis of the molecules is flipped by 180° , it is convenient to consider an order parameter that is invariant under the transformation from e^i to $-e^i$. Explicitly, the order parameter is given by

$$S = \frac{3}{2} \frac{\max_n (N_{e_n} + N_{-e_n})}{\sum_i N_{e^i}} - \frac{1}{2} \quad (2)$$

where N_{e_n} is the number of tiles with orientation e_n and $\sum_i N_{e^i}$ is the total number of particles in the system. The form of the order parameter defined above is so that it lies in the range $[0, 1]$: $S = 1$ indicates perfect orientational order, and $S = 0$ indicates that there is no orientational ordering.

To identify phase transitions, we also calculate the specific heat at constant volume C_V , given by the fluctuation formula:

$$k_B T^2 C_V = \langle (E - \langle E \rangle)^2 \rangle \equiv (\Delta E)^2 \quad (3)$$

where E is the total energy of the system at a given simulation step, given by eq 1, and $\langle E \rangle$ is the average energy calculated over the simulation, after equilibration.

Finally, distinct phases can be characterized and differentiated by their interface extension $\bar{\eta}_I$, given by the average number of empty cells in contact with each tile, and the fraction of accepted MC moves. Compact phases, such as liquid and solid phases, tend to minimize their interface; gas phases and porous materials, such as gels, do not. The fraction of accepted MC moves is, for a lattice system, a measure of the diffusivity of the particles in a certain phase: we expect a lattice gas to be free to translate and rotate, a lattice liquid to have frozen translational degrees of freedom, and a lattice solid to have all of the degrees of freedom frozen.

To characterize the phase transitions and identify the phase boundaries, we monitored the maximum of C_V . Phase transitions may also be associated with a sudden change in the interface extension $\bar{\eta}_I$, a change in the order parameter S , and a change in the number of H-bonds per tile $\bar{\eta}_H$; therefore, the first

derivative and the standard deviation (susceptibility) of these quantities is also useful to determine the phase boundaries. An alternative way to locate the phase boundaries involves the calculation of the chemical potential, but we choose to define the phase boundaries in terms of parameters easily extracted from STM images, such as the orientational order parameter, the interface extension, and the number of hydrogen bonds which define the structural changes associated with the phase transitions identified by the variation of the heat capacity.

3. Results

We performed a set of simulations for every tile in Figure 2, where only two edges are charged with opposite polarity $+q$ and $-q$, to investigate their phase behavior as a function of the bonding parameter q . We investigated values of q from $q = 1$ to $q = 10$. Each simulation was performed at constant density and temperature, using 1250 particles, considering lattice sizes from 36×36 (96% coverage, density $d = 0.96$) to 112×112 (10% coverage, density $d = 0.10$). Periodic boundary conditions have been used. Throughout this section, all of the energies are expressed in units of ϵ , and the reduced temperature is defined as $T^* = k_B T / q^2$.

For every value of q and for every tile type, a chain of simulations was built. Every simulation of the chain was performed at a lower temperature with respect to the previous one. We explored reduced temperatures from 1.0 to 0.001 for tiles A and C and from 0.5 to 0.0005 for tile B. Each chain started with $T^* = 1.0$ (tiles A and C), or $T^* = 0.5$ (tile B), and each successive simulation was run lowering the temperature of the previous simulation by $\Delta T^* = 0.001$ (tiles A and C), or $\Delta T^* = 0.0005$ (tile B). We performed a chain of 1000 simulations, each corresponding to a temperature step. At every temperature step, 10^8 MC moves were attempted, and the resulting configuration was then used as a starting configuration for the next temperature step. In addition, we looked for hysteresis in the phase diagram: we repeated the simulation chains for each tile starting from the lowest temperature end configurations and $T^* = 0.001$ (tiles A and C), or $T^* = 0.0005$ (tile B), and increasing the temperature by $\Delta T^* = 0.001$ (tiles A and C), or $\Delta T^* = 0.0005$ (tile B), at every temperature step. No significant differences were found between the two sets of simulations, and therefore, only results from the cooling cycle will be presented.

To analyze the details of the phase diagrams associated with each particle, we calculated the orientational order parameter S , heat capacity C_V , average number of H-bonds per tile \bar{n}_H , and interface extension \bar{n}_I as a function of T^* , for each tile, and for each function, we calculated the susceptibility ΔX as $\Delta X = \langle X^2 \rangle - \langle X \rangle^2$.

At high temperature, all of the systems show a *gas* phase, in which the tiles are free to move and occupy all of the available volume. At intermediate temperatures, some systems show a *liquid* phase, in which the tiles are packed but not yet frozen in their positions/orientations. At low temperatures, the solid structures that we encountered are illustrated in Figure 3 (and quantitatively discussed in the next section). Each system presents one of five possible solid structures, depending on the value of q ; the possible solid structures are (i) *compact aperiodic*, observed for tile A and small values of q where the tiles form trimers and the trimers pack without forming a periodic structure, (ii) *supramolecular gel*, observed for tile A and large values of q , in which the trimers are arranged into a network that extends to occupy all of the available surface, (iii) *crystal*, formed by both tiles B and C, at low values of q , in

which the tiles appear ordered and well packed, (iv) *gel*, observed for tile B and large values of q , in which we observe a disordered solid arranged into a network that spans all of the available space, and (v) *fibers*, formed by tile C, that at large values of q form elongated structures.

Gels are disordered solids, whose components are arranged into a network, that usually extends to occupy all of the available volume.^{48,49} In the case of tile B, at larger values of q , we observe honeycomb structures and zigzag chains that extend to occupy the whole simulation box. In the case of tile A and large q , the tiles associate into trimers and the trimers form chains which span the whole available space, that is why we call this structure supramolecular gel.

In the rest of this section, first, we analyze the effect of the temperature on each system, and the relative phase diagram, discussing a set of simulations on a 50×50 lattice; then, we analyze the effect of the density on the phase diagrams.

3.1. Effect of the Temperature and Phase Diagrams. Tile

A. The phase diagram for tile A at 50% coverage is shown in Figure 4. In this system, we observe four phases: gas, liquid, compact aperiodic (or solid), and supramolecular gel. The phase boundaries are determined from the maximum of the C_V and the maximum of $\Delta \bar{n}_H$. Interestingly, the phases expressed by tile A are characterized by a lack of orientational order at every temperature ($S \approx 0$, Figure 5b).

At high temperatures, at every value of q , the system behaves like a gas: in this phase, each tile is free to translate and rotate (Figure 5e,f), and the interface extension \bar{n}_I is equal to 3 (Figure 5d), which is the maximum possible value for \bar{n}_I , given that the system coverage is equal to 50% (i.e., if the tiles occupy random sites on the lattice, each tile has on average three occupied and three empty sites in its neighborhood).

As the temperature decreases, the phases encountered by the system depend on the value of q . At low values of q , the system crosses two phase transitions, the highest temperature one characterized by a peak in the C_V and the lowest temperature one by a shoulder in the same parameter (Figure 5a): the first phase transition has an associated change in the interface extension \bar{n}_I (Figure 5d); the second phase transition is instead associated with a peak in $\Delta \bar{n}_H$, a parameter associated with the frequency in which the bonds are broken and formed but also a change in the number of H-bonds per tile \bar{n}_H (Figure 5c), which identify a transition to a solid state. The phase between these two phase transitions is a liquid phase, characterized by the minimization of \bar{n}_I (Figure 5d), a lack of orientational order (Figure 5b), and frozen translational degrees of freedom (Figure 5f). The phase at low temperature corresponds instead to a packed solid, in which all of the motions are frozen (Figure 5e,f). This solid lacks long-range order but presents a local ordering of the tiles, which form trimers that, in turn, are randomly packed (see Figure 3A, left). As q increases, the first phase transition shifts toward lower reduced temperatures (Figure 5a) and, at $q = 1.5$, it overlaps with the second phase transition. At $q = 1.8$, the solid phase is no longer packed, as can be assumed by a smaller decrease of \bar{n}_I at low temperature, with respect to that at lower values of q (Figure 5d). This solid presents the same local structure of the packed solid, namely, it is formed of trimers (see Figure 3A (right)), but the trimers are not closely packed; instead, they are associated to form a supramolecular gel. In this model, the trimers do not diffuse on the surface, unless the trimer is broken. Including the possibility of group moves³⁸ in our model will facilitate the diffusion of the trimers toward each other. Including group moves might be expected to shift the location of the solid/crystal

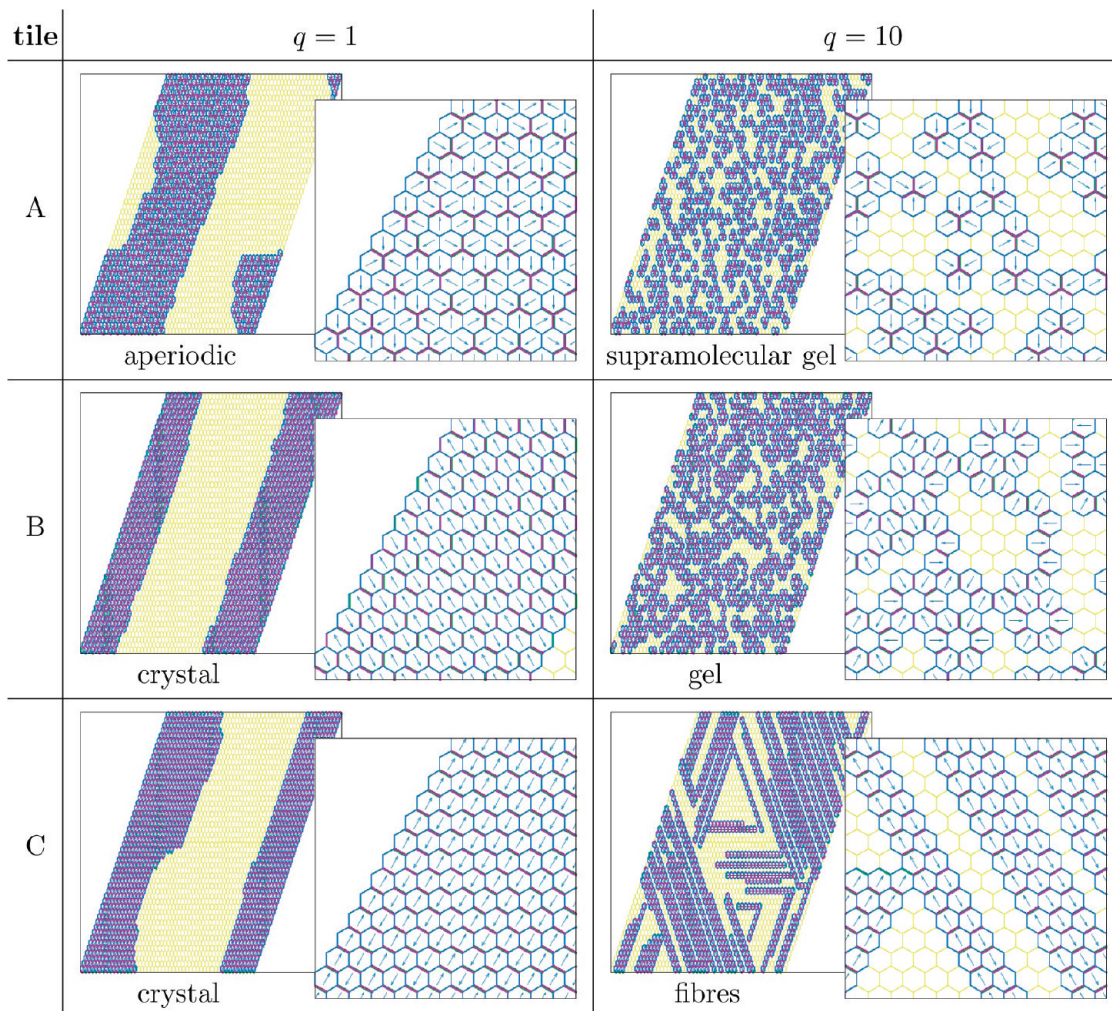


Figure 3. The solid phases obtained at low temperature for systems composed by tiles A, B, and C at 50% coverage ($d = 0.50$) for $q = 1$ and $q = 10$. A magnification of each structure is also shown.

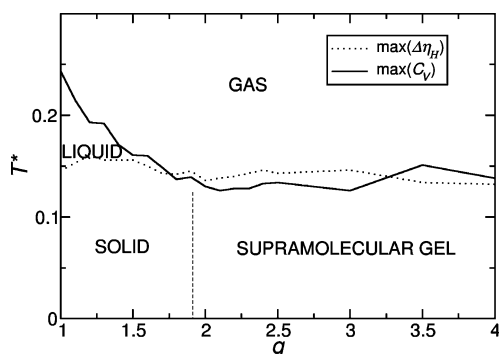


Figure 4. Tile A, phase diagram at 50% coverage. The phase boundaries are identified by the maxima of $\Delta\eta_H$ (dotted line) and C_V (solid line). The vertical dashed line indicates the value of q beyond which no transition is seen in $\bar{\eta}_l$ (see text).

and solid/gel phase boundaries; however, previous studies using MC simulations with group moves have also observed similar kinetically trapped structures.⁵⁰

Tile A, which has the groups with the complementary interactions on two adjacent edges, can therefore pack densely but cannot form ordered structures. As we have shown in Figure 1, the phthalic acid has never been observed forming regular patterns, and CTBPP on Au(111) forms isolated trimers. The packing can be controlled by tuning the energy separation between different sides of the molecule; experimentally, this may be controlled by changing the donor/acceptor groups.

Tile B. The phase diagram for tile B is shown in Figure 6. Tile B shows gas, liquid, crystalline, and gel phases. The gas–liquid transition and the liquid–crystal transition are analogous to that observed for tile A, as can be verified comparing Figures 5 and 7 in the case of $q = 1$. The only difference is that the liquid–crystal phase transition in this system can also be identified by the maximum of ΔS , which takes place at the same point of the maximum of $\Delta\bar{\eta}_H$ (Figure 7b,c).

As for tile A, at low values of q ($q < 1.7$), the system undergoes two phase transitions upon cooling: first a gas–liquid transition, followed by a freezing transition. The freezing transition is associated with a sharp peak in the ΔS . At intermediate values of q ($1.7 \leq q \leq 2.4$), we observe a gas–crystal transition identified by the maximum of ΔC_V and the maximum of ΔS . At higher values of q ($q \geq 2.5$), the gas–gel transition, peculiar of this particular bonding pattern, occurs between the maximum of C_V and the maximum of ΔC_V . With respect to the ongoing discussion on where to place the transition temperature in a gel system, given that different system parameters are modified at different temperatures,⁴⁸ our results suggest that it would be reasonable to define a “transition interval of temperatures”, instead of a single transition temperature. In fact, in this window of temperatures, a sequence of events happens: at higher temperature, C_V reaches its maximum value; here, we also observe the maximum of $\Delta\bar{\eta}_H$ (Figure 7c) and the maximum of the slope of the energy function (not

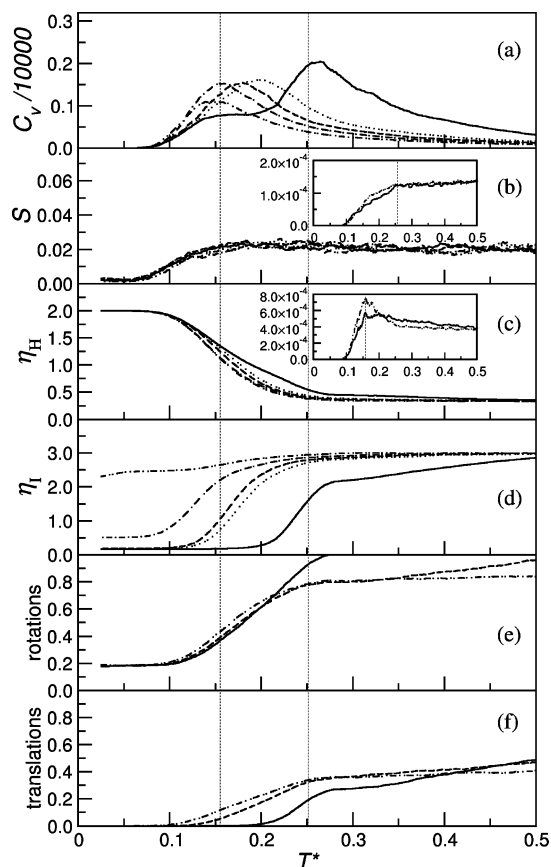


Figure 5. Tile A. (a) Heat capacity C_V , (b) order parameter S , (c) average number of H-like bonds per tile $\bar{\eta}_H$, (d) interface per tile $\bar{\eta}_I$, and (e) accepted rotational and (f) translational moves as a function of the temperature T^* for $q = 1.0$ (solid line), $q = 1.3$ (dotted line), $q = 1.8$ (dashed–dotted line), and $q = 4.0$ (dashed–dotted–dotted line). In the insets: (b) $\Delta S = \langle S^2 \rangle - \langle S \rangle^2$, and (c) $\Delta \eta_H = \langle \eta_H^2 \rangle - \langle \eta_H \rangle^2$. The dashed vertical lines identify the two phase transition temperatures of the system with $q = 1$.

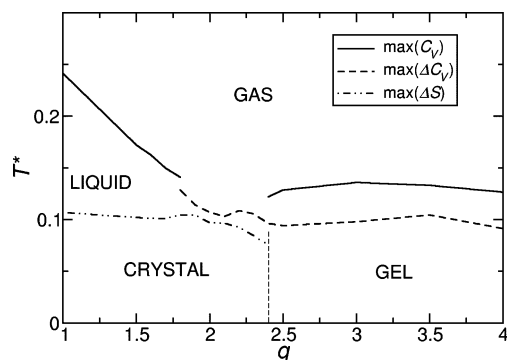


Figure 6. Tile B, phase diagram. The phase boundaries are identified by the maxima of C_V (solid line), ΔC_V (dashed line), and ΔS (dashed–dotted line). The vertical dashed line indicates the value of q beyond which no transition is seen in $\bar{\eta}_I$ (see text).

shown), and at lower temperature, the maximum of the $\Delta \bar{\eta}_I$ (Figure 7d) curve is found at the same temperature of the maximum of the slope of the C_V curve.

An additional feature of this phase diagram is that, as q increases, the gas–liquid phase transition shifts toward lower temperatures (Figure 7a), and, at $q = 1.7$, it overlaps with the liquid–solid phase transition. In this point, we have simultaneous packing and ordering of the system. The low temperature structure we observe is indistinguishable from the crystal structure in Figure 3B. At $q \geq 2.4$, the system is no longer

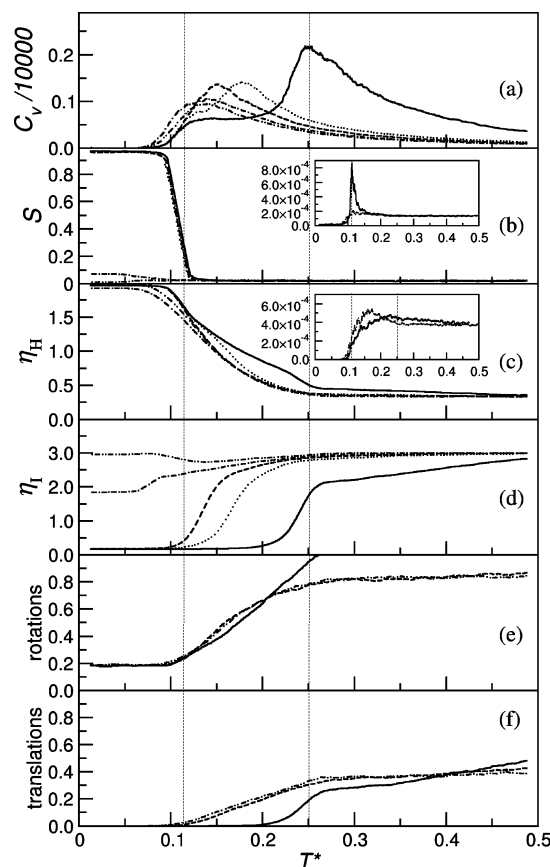


Figure 7. Tile B. (a) Heat capacity C_V , (b) order parameter S , (c) average number of H-like bonds per tile $\bar{\eta}_H$, (d) interface per tile $\bar{\eta}_I$, and (e) accepted rotational and (f) translational moves as a function of the temperature T^* for $q = 1.0$ (solid line), $q = 1.5$ (dotted line), $q = 1.8$ (dashed line), $q = 2.5$ (dashed–dotted line), and $q = 4.0$ (dashed–dotted–dotted line). In the insets: (b) $\Delta S = \langle S^2 \rangle - \langle S \rangle^2$, and (c) $\Delta \eta_H = \langle \eta_H^2 \rangle - \langle \eta_H \rangle^2$. The dashed vertical lines identify the two phase transition temperatures of the system with $q = 1$.

capable, under the chosen simulation conditions, to reach a perfectly ordered state ($S < 1$, at low temperature, Figure 7b), and the single phase transition changes its characteristics: the transition is not anymore associated with a sudden change in S , but it remains associated with a change in $\bar{\eta}_H$. The low temperature structure we observe at $q \geq 2.4$ is the gel structure in Figure 3B (right).

From these results, we argue that molecules with the bonding motif of tile B are likely to be trapped in a gel phase for large values of the complementary bonding strength (q), as happens with the cytosine on Au(111).¹⁹ Unlike tile A, this bonding pattern shows an ordered structure when the energy separation between different sides of the molecule is small, as with the meta-dicarboxylic acid on graphite (Figure 1). Therefore, also in this case, the key to achieve a packed structure is to design the building blocks such that the stronger complementary interactions are not greater than 2.5 times the weaker interactions. This can be achieved not only changing the chemical structure of the molecule but also changing the experimental conditions; for example, cytosine can form ordered structures when deposited in the presence of a solvent.⁵¹

Tile C. The phases we observe for tile C are gas, liquid, crystalline, and fibers (Figure 8). Unlike the previously discussed systems, this system does not present disordered solid phases. At low temperature, the system is aligned at every value of q (Figure 9b). The phase boundaries can be identified plotting the maxima of ΔS and of C_V . Also in this case, as for tile A,

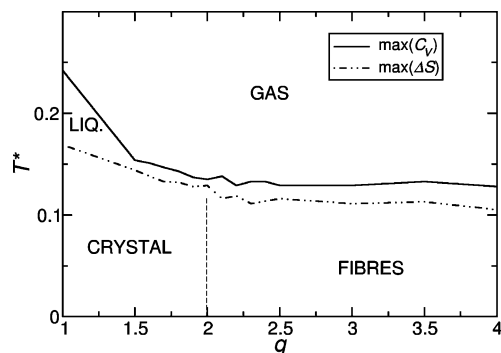


Figure 8. Tile C, phase diagram. The phase boundaries are identified by the maxima of C_V (solid line) and ΔS (dotted–dotted–solid line). The vertical dashed line indicates the value of q beyond which no transition is seen in $\bar{\eta}_I$ (see text), and it is not associated with any phase transition.

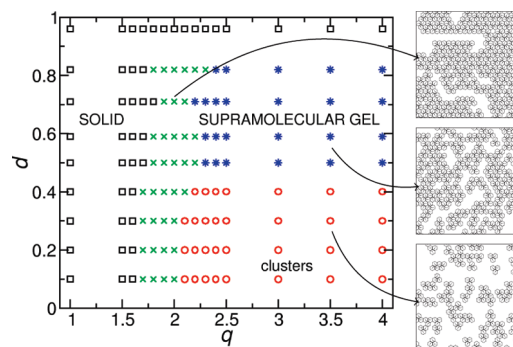


Figure 10. Tile A: d vs q phase diagram, at $T^* = 0.001$. At low temperature, we observe a solid (squares), a supramolecular gel (stars), isolated clusters (circles), or the coexistence of two phases (crosses), depending on the interaction strength q and the system density.

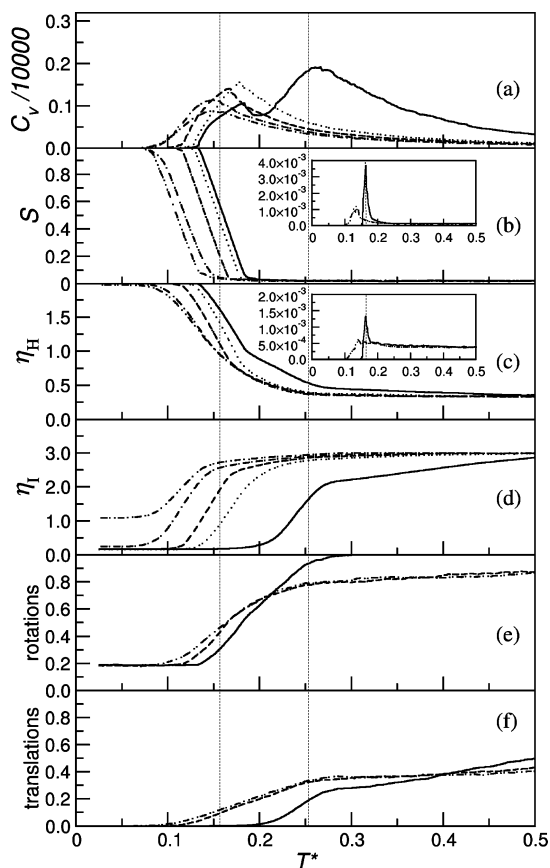


Figure 9. Tile C. (a) Heat capacity C_V , (b) order parameter S , (c) average number of H-like bonds per tile $\bar{\eta}_H$, (d) interface per tile $\bar{\eta}_I$, and (e) accepted rotational and (f) translational moves as a function of the temperature T^* for $q = 1.0$ (solid line), $q = 1.5$ (dotted line), $q = 1.8$ (dashed line), $q = 2.5$ (dashed–dotted line), and $q = 4.0$ (dashed–dotted–dotted line). In the insets: (b) $\Delta S = \langle S^2 \rangle - \langle S \rangle^2$, and (c) $\Delta \eta_H = \langle \eta_H^2 \rangle - \langle \eta_H \rangle^2$. The dashed vertical lines identify the two phase transition temperatures of the system with $q = 1$.

the maximum of ΔC_V is never associated with any other property transition. The gas–liquid and liquid–crystal transitions are analogous to the gas–liquid and liquid–crystal transitions observed for tile B, the first associated with a change in C_V and a drop in η_I , and the second associated with sharp peaks in ΔS and $\Delta \eta_H$. However, the gas–fibers transition has its own characteristics and it appears to happen in two steps: at higher temperature, the H-bonds are formed (Figure 9c) and this corresponds to the maximum of C_V (Figure 9a); at lower

temperature, the interface extension is minimized (Figure 9d) and this corresponds to the maximum of ΔS (Figure 9b). The high temperature part of this phase transition is analogous to that of the gas–gel transition of tile B. The low temperature part of the phase transition is different because there is a variation of the orientational order parameter S , but the change in the second derivative of C_V which, in this case, appears at even lower temperatures, is not associated with any other property change (not shown). In comparison with tiles A and B, the liquid phase is stable over a much smaller region of the phase diagram.

Another feature that differentiates tile C from tiles A and B is that, in this case, both phase transitions shift toward lower temperatures as q increases, as indicated by a shift of both the average number of H-bonds per tile (Figure 9c) and the orientational order parameter S (Figure 9b). At $q > 2$, under the current simulation conditions, the system is not able to minimize the interface extension (Figure 9d).

The H-bond strength can therefore be tuned to switch between a packed solid and fibers (as in Figure 3C). The bonding strength is not, however, the only parameter that needs to be tuned. As we will see in the following section, the lattice coverage turns out to be an important controlling parameter in the fibers formation.

3.2. Effect of the Lattice Coverage. To study the effect of the lattice coverage, we performed a set of simulations at constant density, using 1250 particles, considering lattice sizes from 36×36 (96% coverage, density $d = 0.96$) to 112×112 (10% coverage, density $d = 0.10$). We rationalize here the end simulation configurations ($T^* = 0.001$ for tiles A and C and $T^* = 0.0005$ for tile B) in a set of three phase diagrams.

Tile A. As previously pointed out, the tile A solid structures consist of the assembly of trimers (as in Figure 3A) which can form a packed solid or a supramolecular gel (Figure 10). The density does not have any effect on the packed solid observed at low q ($q \leq 1.6$), but it does affect the nonpacked structures observed at higher values of q . Due to the limited system size, we are unable to identify accurate phase boundaries; however, we can identify the typical behavior observed in systems that present gel phases:⁴⁸ at low densities ($d < 0.5$), we observe isolated clusters, and at high densities, we observe a gel that spans all of the available space. At intermediate values of q , we generally observe coexistence of the packed and nonpacked structures, which usually appears as isolated trimers coexisting with a wide surface occupied by the solid. The lack of a packed structure over a wide range of q for this bonding pattern is

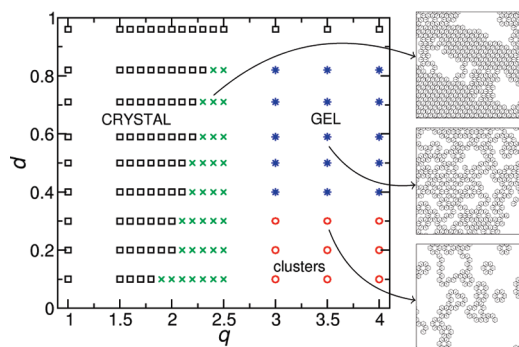


Figure 11. Tile B: d vs q phase diagram, at $T^* = 0.0005$. At low temperature, we observe a crystal (squares), a gel (stars), isolated clusters (circles), or the coexistence of two phases (crosses), depending on the interaction strength q and the system density.

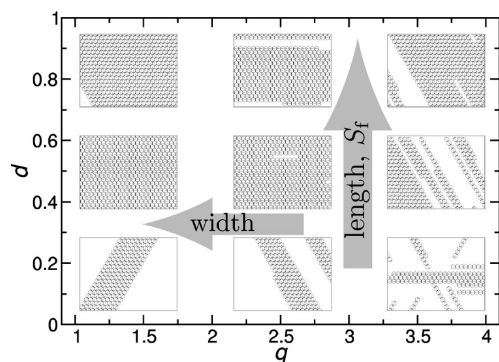


Figure 12. Tile C: d vs q scheme, at $T^* = 0.001$. At low temperature, we observe different fiber conformations depending on the interaction strength and the system density. The vertical and horizontal arrows indicate the direction of increasing fiber lengths and of increasing fiber widths, respectively.

consistent with STM studies on phthalic acid⁶ and other molecules.^{17,18}

Tile B. The phase diagram for tile B (Figure 11) is analogous to that of tile A as three phases are observed, with a coexistence region. The differences are that isolated clusters are observed at low densities, where the building blocks assemble into hexamers and chains, and the gel appears at lower densities ($d > 0.3$) with respect to what is observed for tile A. The region of coexistence between the crystal and the nonpacked structures is pushed toward higher densities as q increases. For example, at $q = 2.2$, the two solid phases, disordered gel and ordered crystal, coexist. Thus, it is possible to obtain a packed structure through increasing density. This is not the case if $q > 2.3$: here, we observe the coexistence of crystal and gel at every density. These results partially explain why a density increase is sometimes insufficient to promote ordered structures, as happens with the cytosine deposition on Au(111)¹⁹ where cytosine molecules are arranged in a disordered structure even when the coverage is increased (see Figure 1e).

Tile C. For tile C, it is not possible to draw a phase diagram as for the other two systems. The transition between the observed structures occurs smoothly through the entire range of explored parameters. In this system (Figure 12), at low q and high d we observe a crystalline structure and at high q and low density we observe short unidimensional fibers. It is possible however to characterize the fibers through their width and length. Moreover, as the fibers are formed by unidimensional fibrils, composed by isoaligned tiles connected through their charged edges, it is possible to assign a direction to each fibril and

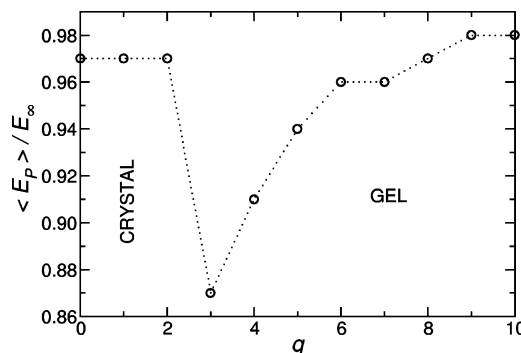


Figure 13. Tile B. The ratio $\langle E_P \rangle / E_\infty$ is plotted against q .

calculate a fibril order parameter S_f as in eq 2. The fibers elongate and align when the system density is increased, and their width increases as the complementary interaction strength decreases.

The results for tile C suggest that fiber morphology is affected by the interplay between complementary interactions and sample density. Moreover, as for tile B, if the desired result is a crystal, an increase in density is not enough to achieve such a structure if the complementary interactions are too strong (e.g., $q > 2$).

4. Discussion and Conclusion

In this paper, we discussed a 2D lattice model for the study of hydrogen-bonded molecular networks deposited on a surface which brings into a unified framework the different structures that one can encounter with the most common bonding motifs. The model is able to reproduce the experimentally observed crystalline compact structure and three experimentally observed noncompact structures (gel, colloidal gel, and fibers). It also predicts an aperiodic compact structure not yet reported by the experiments. Moreover, our model shows how changes in the bonding strength of the building blocks can be used to control the transition between gel/colloid/fibers states and compact phases: as the separation between the energies increases, it is more difficult to get the lowest energy configuration, in agreement with the experiments.⁵² The algorithm we employed is based on single particle moves (where group moves are not allowed). The inclusion of group moves³⁸ is expected to affect the phase diagrams moving the phase boundary between compact and noncompact structures toward higher values of q .

To understand why these particles do not form a packed structure at zero temperature and every value of q , we focus our attention on tile B of Figure 2, in the case of $d = 0.50$, and we calculate the average energy per particle ($\langle E_P \rangle = \langle E \rangle / N$) in the simulated system, and, as a reference, the energy per particle (E_∞) for an infinite regular solid (density $d = 1.00$). Given that each tile can interact with six neighbors with van der Waals-like interaction and with two tiles with an electrostatic contribution, we get

$$E_\infty = -(3 + q^2) \quad (4)$$

The ratio $\langle E_P \rangle / E_\infty$, plotted in Figure 13, has an interesting behavior as a function of q : the ratio falls suddenly from ~ 0.97 to ~ 0.87 as q increases, and slowly it recovers to 0.98 . In all cases, the ratio is not unitary because of the effect of the interface. This result suggests that, at high values of q ,

a less packed structure is most likely to appear as it is energetically favorable to form extended structures to maximize the electrostatic interaction, at the cost of decreasing the nonspecific interaction due to the van der Waals interactions. The gel structure, even if higher energy with respect to packed structures, may also be expected to be stabilized by entropic contributions, which contribute to lowering the free energy of the system.

It should be noted that the present model assumes each molecule occupies a single lattice site. While this is a good approximation for many experimental systems, in other cases, a molecule will occupy a number of adjacent lattice sites. This extended, excluded volume effect has been shown, even in the case of purely repulsive interactions, to lead to a rich phase behavior.⁵³

Despite its simplicity, the proposed model can be related to and is consistent with the experimental observations. For example, meta- and para-benzene-dicarboxylic acids form regular patterns, while the ortho has never been observed forming regular structures.⁶ To connect our model with realistic energy values, it is possible to proceed as follows. Given that, in our model, two charged edges interact with $E_{\text{strong}} = -(\epsilon + q^2)$ and two noncharged edges interact with $E_{\text{weak}} = -\epsilon$, and all of the energies are expressed in units of ϵ , the value of q can be calculated as $|E_{\text{strong}} - E_{\text{weak}}|/E_{\text{weak}}^{1/2}$, where E_{strong} is referred to the strongest binding energy (e.g., the energy related to the H-bonded configuration) and E_{weak} to the weaker (e.g., the van der Waals energy of two molecules non-H-bonded). The values for E_{strong} and E_{weak} can be calculated with molecular mechanics methods or taken from the literature. For example, calculations using the MM3 force field show that the meta-benzene-dicarboxylic acid, which has the bonding pattern of tile B, has $E_{\text{weak}} = -1.72$ kcal/mol and $E_{\text{strong}} = -11.16$ kcal/mol which corresponds to $q = 2.34$, and forms a regular structure, in agreement with the experiments.⁶ Cytosine interaction energies can instead be found in the literature.⁵⁴ Using the estimates of ref 54 ($E_{\text{weak}} \approx 0.05E_{\text{strong}}$ with $E_{\text{strong}} = -20.7$ kcal/mol), we get $q \approx 4.36$. The cytosine also presents the same bonding pattern of tile B, and its value of q corresponds to the formation of a 2D gel, which is in agreement with the experiment.¹⁹

This model can be therefore considered intermediate between a purely phenomenological (qualitative) model and a quantitative (atomistic) description of the patterns formed by H-bonded molecules. As the full characterization of the phase diagram is too computationally expensive for an atomistic study, we suggest that a simulation approach like the one proposed here is the most suitable to rationalize the vast amount of experimental information available.

Acknowledgment. The authors wish to acknowledge useful conversations with Professor Michael P. Allen. We are grateful to the Leverhulme Trust and EPSRC for financial support. Computing facilities have been provided by the Centre for Scientific Computing, University of Warwick.

References and Notes

- (1) Tomba, G.; Vita, A. D. *Adv. Mater.* **2009**, *21*, 1055–1066.
- (2) Feyter, S. D.; Schryver, F. C. D. *Chem. Soc. Rev.* **2003**, *32*, 139–150.
- (3) Barth, J. V.; Costantini, G.; Kern, K. *Nature* **2005**, *437*, 671–679.
- (4) Stepanow, S.; Lin, N.; Vidal, F.; Landa, A.; Ruben, M.; Barth, J. V.; Kern, K. *Nano Lett.* **2005**, *5*, 901–904.
- (5) Dou, W.; Guan, D.; Mao, H.; Song, F.; Huang, H.; Zhang, H.; Li, H.; He, P.; Bao, S. *Chem. Phys. Lett.* **2009**, *470*, 126–130.
- (6) Lackinger, M.; Griessl, S.; Markert, T.; Jamitzky, F.; Heckl, W. M. *J. Phys. Chem. B* **2004**, *108*, 13652–13655.
- (7) Heininger, C.; Kampschulte, L.; Heckl, W. M.; Lackinger, M. *Langmuir* **2009**, *25*, 968–972.
- (8) Zhu, N.; Osada, T.; Komeda, T. *Surf. Sci.* **2007**, *601*, 1789–1794.
- (9) Kwon, K.-Y.; Lin, X.; Pawin, G.; Wong, K.; Bartels, L. *Langmuir* **2006**, *22*, 857–859.
- (10) Miyashita, N.; Kurth, D. G. *J. Mater. Chem.* **2008**, *18*, 2636–2649.
- (11) Xiao, W.; Feng, X.; Ruffieux, P.; Gröning, O.; Müllen, K.; Fasel, R. *J. Am. Chem. Soc.* **2008**, *130*, 8910–8912.
- (12) Madueno, R.; Raisanen, M. T.; Silien, C.; Buck, M. *Nature* **2008**, *454*, 618.
- (13) Theobald, J. A.; Oxtoby, N. S.; Phillips, M. A.; Champness, N. R.; Beton, P. H. *Nature* **2003**, *424*, 1029–1031.
- (14) Zwaneveld, N. A. A.; Pawlak, R.; Abel, M.; Catalin, D.; Gírges, D.; Bertin, D.; Porte, L. *J. Am. Chem. Soc.* **2008**, *130*, 6678–6679.
- (15) Yau, S.; Lee, Y.; Chang, C.; Fan, L.; Yang, Y.; Dow, W.-P. *J. Phys. Chem. C* **2009**, *113*, 13758–13764.
- (16) Fendt, L.-A.; Stoehr, M.; Wintjes, N.; Enache, M.; Jung, T. A.; Diederich, F. *Chemistry* **2009**, *15*, 11139–11150.
- (17) Wang, Y.; Ge, X.; Schull, G.; Berndt, R.; Bornholdt, C.; Herges, F. K. R. *J. Am. Chem. Soc.* **2008**, *130*, 4218–4219.
- (18) Yokoyama, T.; Yokoyama, S.; Kamikado, T.; Okuno, Y.; Mashiko, S. *Nature* **2001**, *413*, 619–621.
- (19) Otero, R.; Lukas, M.; Kelly, R. E. A.; Xu, W.; Laegsgaard, E.; Stensgaard, I.; Kantorovich, L. N.; Besenbacher, F. *Science* **2008**, *319*, 312–315.
- (20) Perdigão, L. M.; Saywell, A.; Fontes, G. N.; Staniec, P. A.; Goretzki, G.; Phillips, A. G.; Champness, N. R.; Beton, P. H. *Chemistry* **2008**, *14*, 7600–7607.
- (21) Clair, S.; Pons, S.; Seitsonen, A. P.; Brune, H.; Kern, K.; Barth, J. V. *J. Phys. Chem. B* **2004**, *108*, 14585–14590.
- (22) Silly, F.; Shaw, A. Q.; Castell, M. R.; Briggs, G. A. D.; Mura, M.; Martsinovich, N.; Kantorovich, L. *J. Phys. Chem. C* **2008**, *112*, 11476–11480.
- (23) Mura, M.; Martsinovich, N.; Kantorovich, L. *Nanotechnology* **2008**, *19*, 465704.
- (24) Okuno, Y.; Yokoyama, T.; Yokoyama, S.; Kamikado, T.; Mashiko, S. *J. Am. Chem. Soc.* **2002**, *124*, 7218–7225.
- (25) Rapino, S.; Zerbetto, F. *Langmuir* **2005**, *21*, 2512–2518.
- (26) Klappenberger, F.; nas Ventura, M. E. C.; Clair, S.; Pons, S.; Schlickum, U.; Qu, Z.-R.; Strunskus, T.; Comisso, A.; Wöll, C.; Brune, H.; Kern, K.; Vita, A. D.; Ruben, M.; Barth, J. V. *ChemPhysChem* **2008**, *9*, 2522–2530.
- (27) Silly, F.; Weber, U. K.; Shaw, A. Q.; Burlakov, V. M.; Castell, M. R.; Briggs, G. A. D.; Pettifor, D. G. *Phys. Rev. B* **2008**, *77*, 201408.
- (28) Kampschulte, L.; Werblowsky, T. L.; Kishore, R. S. K.; Schmitt, M.; Heckl, W. M.; Lackinger, M. *J. Am. Chem. Soc.* **2008**, *130*, 8502–8507.
- (29) Weber, U. K.; Burlakov, V. M.; Perdigão, L. M. A.; Fawcett, R. H. J.; Beton, P. H.; Champness, N. R.; Jefferson, J. H.; Briggs, G. A. D.; Pettifor, D. G. *Phys. Rev. Lett.* **2008**, *100*, 156101.
- (30) Velichko, Y. S.; Stupp, S. I.; Olvera de la Cruz, M. *J. Phys. Chem. B* **2008**, *112*, 2326.
- (31) Wilson, M. R. *Chem. Soc. Rev.* **2007**, *36*, 1881–1888.
- (32) Doye, J. P. K.; Louis, A. A.; Lin, I.-C.; Allen, L. R.; Noya, E. G.; Wilber, A. W.; Kok, H. C. K.; Lyus, R. *Phys. Chem. Chem. Phys.* **2007**, *9*, 2197–2205.
- (33) Binder, K.; Paul, W. *Macromolecules* **2008**, *41*, 4537–4550.
- (34) Swetnam, A. D.; Allen, M. P. *Phys. Chem. Chem. Phys.* **2009**, *11*, 2046–2055.
- (35) Paez, A.; Tarazona, P.; Mateos-Gil, P.; Velez, M. *Soft Matter* **2009**, *5*, 2625–2637.
- (36) Pasini, P.; Chiccoli, C.; Zannoni, C. In *Advances in the Computer Simulation of Liquid Crystals*; Pasini, P., Zannoni, C., Eds.; Kluwer: Dordrecht, The Netherlands, 2000; p 99.
- (37) Jeon, Y. J.; Bingzhu, Y.; Rhee, T. R.; Cheung, D. L.; Jamil, M. *Macromol. Theory Simul.* **2007**, *16*, 643–659.
- (38) Troisi, A.; Wong, V.; Ratner, M. *Proc. Natl. Acad. Sci. U.S.A.* **2005**, *102*, 255–260.
- (39) Jankowski, E.; Glotzer, S. C. *J. Chem. Phys.* **2009**, *131*, 104104/1–8.
- (40) Joknys, A.; Tornau, E. E. *J. Magn. Magn. Mater.* **2009**, *321*, 137–143.
- (41) Salas, J. *J. Phys. A: Math. Gen.* **1998**, *31*, 5969–5980.
- (42) Yeomans, J. *Statistical Mechanics of Phase Transitions*; Oxford Science Publications: Oxford, 1992.
- (43) Higo, J.; Endo, S.; Nagayama, K. *Chem. Phys. Lett.* **1992**, *198*, 300.
- (44) Hoggoku, M. *Adv. Biophys.* **1997**, *34*, 55.
- (45) Bianchi, E.; Largo, J.; Tartaglia, P.; Zaccarelli, E.; Sciortino, F. *Phys. Rev. Lett.* **2006**, *97*, 168301.
- (46) Landau, D.; Binder, K. *A guide to Monte Carlo Simulations in Statistical Physics*; Cambridge University Press: Cambridge, 2000.

- (47) Zwanzig, R. *J. Chem. Phys.* **1963**, *39*, 1714–1719.
- (48) Krzakala, F.; Tarzia, M.; Zdeborova, L. *Phys. Rev. Lett.* **2008**, *101*, 165702.
- (49) Lu, P. J.; Zaccarelli, E.; Ciulla, F.; Schofield, A. B.; Sciortino, F.; Weitz, D. A. *Nature* **2008**, *453*, 499–U4.
- (50) Zaccarelli, Emanuela. *J. Phys.: Condens. Matter* **2007**, *32*, 323101.
- (51) Tao, N. J.; DeRose, J. A.; Lindsay, S. M. *J. Phys. Chem.* **1993**, *97*, 910.
- (52) Lackinger, M.; Griessl, S.; Heckl, W. M.; Hietschold, M.; Flynn, G. W. *Langmuir* **2005**, *21*, 4984–4988.
- (53) Fernandes, H. C. M.; Arenzon, J. J.; Levin, Y. *J. Chem. Phys.* **2007**, *126*, 114508.
- (54) Kelly, R. E. A.; Lukas, M.; Kantorovich, L. N.; Otero, R.; Xu, W.; Mura, M.; Laegsgaard, E.; Stensgaard, I.; Besenbacher, F. *J. Chem. Phys.* **2008**, *129*, 184707.

JP9098649